Journal of Alloys and Compounds 791 (2019) 674–680

Contents lists available at ScienceDirect

Journal of Alloys and Compounds

journal homepage: http://www.elsevier.com/locate/jalcom

Influence of aging on electrocaloric effect in Li^+ doped $BaTiO_3$ ceramics

C. Meric Guvenc, Umut Adem*

Department of Materials Science and Engineering, İzmir Institute of Technology, Urla 35430, İzmir, Turkey

ARTICLE INFO

Article history:
Received 11 November 2018
Received in revised form
25 March 2019
Accepted 26 March 2019
Available online 27 March 2019

Keywords:
Aging
Electrocaloric effect
Defect dipoles
Li-doping
$BaTiO_3$

ABSTRACT

Aging creates significant changes in the properties of the ferroelectric materials such as dielectric and piezoelectric properties. However, the influence of aging on the electrocaloric effect (ECE) has not yet been investigated. In this work, we investigate the effect of the aging on the ECE in acceptor (Li^+) doped $BaTiO_3$ ceramics. We observe that aging induced defect polarization (P_D) reduces the saturation polarization of the doped samples until $T_c = 115\,^{\circ}C$. Above that temperature P_D loses its effectiveness and material behaves like a fresh sample. Suppression of polarization below T_C due to aging effect results in a sharper slope change in the temperature dependence of electrical polarization in aged samples which causes an increase in the electrocaloric temperature change of Li^+ doped $BaTiO_3$ ceramics up to 23% at T_C. Above a critical Li doping amount, both negative and positive electrocaloric effect are observed in the same sample.

1. Introduction

Electrocaloric effect can be described as the adiabatic temperature change of dielectric materials under applied electric field [1–4]. Electrocaloric cooling based on electrocaloric effect is a promising technology which has the potential to replace conventional coolers based on vapor compression [1,4]. Among different types of caloric materials (i.e. magnetocalorics, barocalorics, elastocalorics and electrocalorics) considered for novel solid state cooling devices, electrocaloric materials are shown to be most promising [5]. Even though the cooling characteristics of electrocaloric cooling devices do not yet meet the requirements needed for practical applications, numerical models of device prototypes are being simulated and experimentally validated [6,7]. Mischenko et al. reported a giant electrocaloric effect in antiferroelectric $PbZr_{0.95}Ti_{0,05}O_3$ thin films under 780 kV/cm electric field with 12 K electrocaloric temperature change [8]. After that work, electrocaloric materials have received great attention. Due to the toxicity of lead, lead-free ferroelectric materials especially $BaTiO_3$ and $BaTiO_3$ based systems received more attention because of their excellent ferroelectric properties and relatively high electrocaloric temperature change (ΔT) [9–16]. Moya et al. [9] studied single crystal $BaTiO_3$ samples using both direct and indirect methods, and reported a ΔT of 1.0 K at the ferroelectric (FE) to paraelectric (PE) phase transition. To obtain a relatively high electrocaloric effect in wide temperature range, doping strategies have been extensively studied [10,14,15,17–20]. Many of these studies focus on bringing different ferroelectric phases of $BaTiO_3$ close to each other, thereby making more polarization directions available and reducing the energy barriers required for the polarization of the material [10,14,15,17]. Mostly isovalent doping is used and common dopants are Sr^{2+} and Ca^{2+}at the A-site and Zr^{4+}, Hf^{4+}, Sn^{4+} and Ce^{4+} at the B-site of the perovskite structure [10,13,14,17,21–27]. On the other hand, heterovalent doping has not received as much interest as isovalent substitution. In heterovalent substitution, the dopant atom can occupy either A or B-site. Atoms which have low valence and large atomic radius prefer to occupy the A-site, on the other hand, atoms with high valence and small atomic radius prefer the B-site. Influence of different heterovalent dopants (Mn and some rare-earth elements) on electrocaloric effect have been studied [17,28,29]. Even though there are quite a few studies on Li doping of $BaTiO_3$, influence of Li doping on electrocaloric properties has not been reported so far. Previously, it was reported that the site which Li^+ will choose to occupy is difficult to determine because the ionic radius of Li^+ is close to Ba^{2+} in 12-fold ($r_{Li^+} = 1.18$ Å) coordination and close to Ti^{4+} in 6-fold ($r_{Li^+} = 0.76$ Å) coordination [30,31]. Lou et al. [32] reported that Li^+ first occupies A-site up to a certain Li amount and reaches the limit of the solid solution. Above this

* Corresponding author.
E-mail address: umutadem@iyte.edu.tr (U. Adem).

https://doi.org/10.1016/j.jallcom.2019.03.356
0925-8388/

amount, a large amount of Li^+ occupies the B-site such that eventually both A and B-sites are occupied. Heterovalent doping causes defect formation (oxygen or cation vacancies) in the structure. In the case of acceptor doping, doping induced defect dipole formation changes the ferroelectric and piezoelectric behavior. For example, acceptor Li-doped BT systems show anti-ferroelectric like behavior because of the pinching effect of the defect dipoles [32,33]. Regarding the influence of defects on ECE, computational studies show that defect structures do not constitute an obstacle for the ECE and with the right strategies ECE can be improved [34,35]. Experimentally, the effect of defect polarization on the electrocaloric effect has only recently been demonstrated [36–39]. In $Pb(Zr,Ti)O_3$ ferroelectric bilayer thin films, it was reported that defect polarization induced pinching in the hysteresis loops gradually disappear with increasing temperature, resulting in both negative and positive electrocaloric effect [36]. In another study on ferroelectric $PbZrO_3$ thin films, electrocaloric effect measured by indirect method was shown to depend on the measurement frequency due to the defect-related polarization switching dynamics [37]. In Mn-doped $Pb(In_{0.5}Nb_{0.5})O_3$–$PbTiO_3$ ceramics, defect dipoles induced by Mn-doping significantly changes the electrocaloric effect compared to the undoped sample, resulting in both positive and negative electrocaloric effect [38]. In a study on Fe-doped $Pb(Zr,Ti)O_3$ ferroelectric ceramics, it was shown that the electrocaloric effect depends on poling direction since the poling direction controls the internal bias field caused by defect dipoles [39]. Despite these studies about the effect of defect polarization on the electrocaloric effect, the effect of aging on the electrocaloric effect has not been described systematically.

Aging effect can be defined as the time-dependent change of ferroelectric, dielectric and piezoelectric properties [40–46]. It is believed that the aging behavior is caused by the symmetry conforming short range ordering (SC-SRO) tendency of point defects to comply with general crystal symmetry [40]. Also, it is known that the acceptor doping strongly contributes to the aging effect of the ferroelectric materials [40–42,44,45]. Acceptor doping induces the formation of oxygen vacancies which constitute a defect dipole together with the acceptor dopant. In general, the aging behavior is thought to be related with the time dependent oxygen vacancy migration in acceptor-doped ferroelectrics. However, the source of the activation energy for oxygen vacancy migration is still a matter of debate [44,45]. Aging behavior can be considered as undesirable behavior because it affects the stability and reliability of the material [47]. However, recent studies have shown that aging causes high and repeatable electrostrain in unpoled acceptor-doped $BaTiO_3$ single crystals [48,49] and polycrystals [50].

In this study, we demonstrate the effect of aging on the ferroelectric and electrocaloric properties of the Li^+ doped $BaTiO_3$ (LBT) ceramics, with different Li^+ doping amounts: 4% (LBT4), 6% (LBT6) and 8% (LBT8). We show that electrocaloric temperature change of the aged samples increases at T_C due to influence of the defect dipoles and this contribution might even result in negative electrocaloric effect.

2. Experimental

The conventional solid state synthesis was used to synthesize Li^+-doped $BaTiO_3$ samples. Firstly, stoichiometric $BaTiO_3$ powder is synthesized using high purity $BaCO_3$ (>99.5%, Enteknomaterials) and TiO_2 (>99.5%, Enteknomaterials). The powders were mixed in ethanol media for 18 h using a planetary ball mill (Retsch PM 100) in high density polyethylene jar with yttria-stabilized zirconia balls. The mixture was dried and then calcined at 1000 °C for 5 h in air. A known amount of Li_2CO_3 (4–8% mole percent) (99.999%, Sigma-Aldrich), $BaTiO_3$ and (2.0% (w/t)) PVA as binder were added to distilled water. This suspension was mixed in the planetary ball-mill for 18 h. After that, the mixture was dried, sieved and uniaxially pressed into disc-shaped samples. Binder burnout was carried out at 600 °C for 5 h with a heating rate of 1 °C/min. Then, the samples were sintered at 1200 °C for 5 h with 5 °C/min heating rate. The bulk sample densities were measured using the Archimedes method. Powder X-ray diffraction (PXRD) measurements were done using a Rigaku Miniflex 600 with Cu K_α radiation. Profile fitting of the XRD patterns was carried out using GSAS-II software [51]. The microstructure and grain size were analyzed on thermally etched samples using a scanning electron microscope (SEM) (Philips XL 30SFEG). To measure the electrical properties, sintered pellets were polished down to a thickness of 1.0 mm. Then, silver paste was coated on both surfaces of the samples to form contacts. Dielectric constant was measured by a precision LCR meter (Keysight Technologies E4980AL) from 40 to 200 °C at 1 kHz. Ferroelectric hysteresis loops were measured using a Ferroelectric Analyzer (AixACCT TF1000), at 10 Hz between 30°-150 °C. For aging experiments, first a fresh state is assured by holding the samples at 200 °C for one day and then air quenching to room temperature and ferroelectric hysteresis loops are measured immediately after. To obtain the aged samples, measured fresh samples were kept at room temperature for ten days and P-E hysteresis loops were measured again at 10 Hz between 30°-150 °C.

3. Results and discussion

3.1. Microstructural characterization

XRD patterns of sintered BT and LBT samples at the room temperature are shown in Fig. 1. All samples have pure perovskite structure without any impurity phases, implying that all dopants are incorporated into the perovskite structure. BT sample sintered at the same temperature as LBT samples doesn't show any peak splitting, implying cubic symmetry. On the other hand, LBT samples showed peak splitting of the (002) and (200) peaks around 45° and the ratio of (200) to (002) is greater than 1, indicating tetragonal crystal structure. We also observe changes in tetragonality with Li doping. c/a values obtained from profile fitting of the XRD data (Pawley fits are provided in the Supplementary Information File) are 1.0056, 1.0068 and 1.0058 for LBT4, LBT6 and LBT8 samples, respectively.

SEM images of sintered LBT ceramics are presented in Fig. 2. As can be seen from the microstructures, all samples are dense and do not contain any secondary phases. According to SEM micrographs

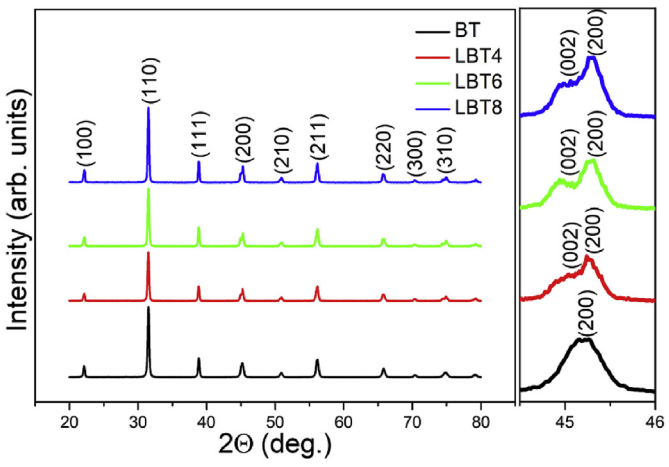

Fig. 1. XRD patterns for BT and LBT ceramics with different Li^+ concentration.

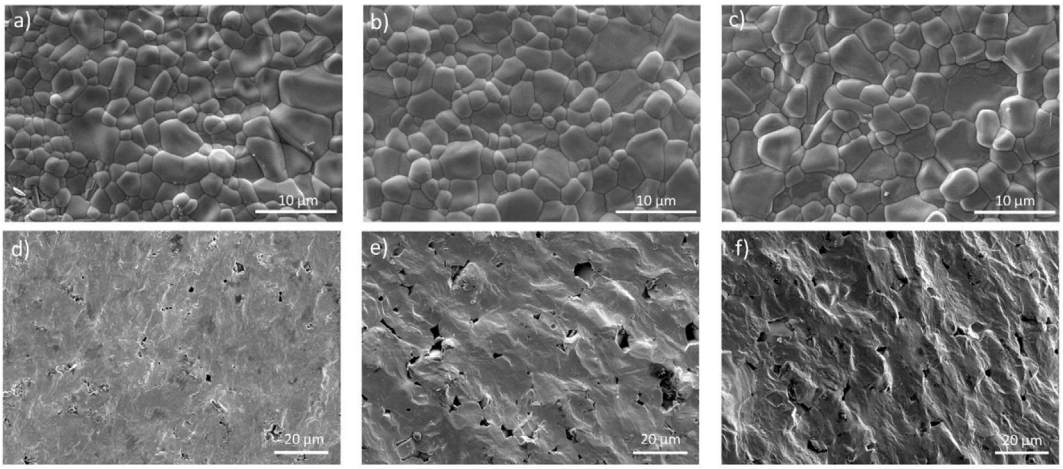

Fig. 2. SEM images for LBT4, LBT6, LBT8 ceramics. (a), (b), (c): polished and thermally etched surfaces. (d), (e), (f): fracture surfaces.

showing surface images in Fig. 2(a–c), with increasing Li^+ content, average grain size of LBT ceramics increases. Careful application of the linear intercept method yielded average grain sizes of 2.25, 2.64 and 2.95 μm for LBT4, LBT6 and LBT8 samples, respectively. This increase in grain size can be associated with the oxygen vacancy formation as the acceptor doping creates oxygen vacancies in the system. Oxygen vacancies can promote sintering behavior and mass transport, resulting in a larger grain size as reported earlier [30]. SEM images from the fracture surfaces are presented in Fig. 2(d–f). The images reveal that these samples had trans-granular fracture which indicates that the internal binding forces between the grains are smaller than those forces between the grain boundaries. This implies that Li^+ ions occupy the lattice sites without any segregation at the grain boundaries. It should be noted that the segregation may cause weakening at the grain boundaries.

3.2. Dielectric measurements

The temperature dependence of the dielectric constant of LBT ceramics measured at 1 kHz frequency is shown in Fig. 3. All specimens show a sharp dielectric peak at the Curie temperature

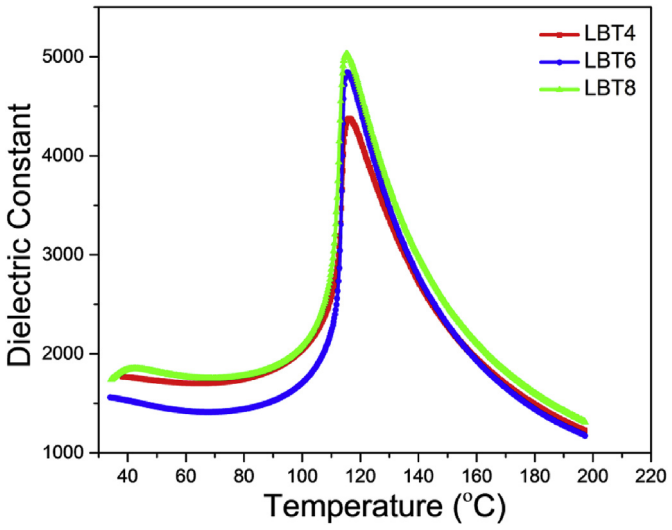

Fig. 3. The temperature dependence of the dielectric constant at 1 kHz for the LBT4, LBT6, LBT8 ceramics.

which implies a first order phase transition. Dielectric peak was observed approximately at 115 °C for all Li^+ doped compositions. Dielectric peak value increases significantly from LBT4 sample to LBT6 sample while the increase from LBT6 to LBT8 sample is minor. This increase can be correlated with the increase in the grain size (2.25, 2.64 and 2.95 μm for LBT4, LBT6 and LBT8 samples, respectively) of the samples with Li doping [52].

3.3. Aging and electrocaloric effect

Fig. 4 shows P-E loops of fresh and aged samples at different temperatures between 30° and 150 °C. Firstly, at 30 °C, all fresh samples demonstrated regular hysteresis loops. Loops become pinched with the increase of temperature until below *Tc*. When the temperature approaches T_C, pinching effect disappears and above T_C, as the material becomes paraelectric, we observe linear hysteresis loops. Pinching in the loops become more evident with the increase of Li^+ amount. Additionally, we observe development of asymmetry in hysteresis loops with increasing temperature for the fresh samples: The first hysteresis measurement at 30 °C yields almost symmetric hysteresis loop for all LBT compositions; however, as the temperature is increased, the loops shift towards left progressively until the temperature approaches the Curie temperature. Close to the Curie temperature and above, loops become symmetric again. Actually, fresh samples also age as the temperature is increased during the hysteresis measurement as can be inferred from the increasing pinching and asymmetry in the loops with increasing temperature. The accelerating effect of the temperature on aging is well-known [53]. However, since aging is a time dependent process and it is not complete, we still refer to these samples as 'fresh' samples.

On the other hand, aged LBT samples show major changes in the hysteresis loops. Remanent polarization of all aged LBT samples decreases quite significantly compared to their fresh LBT counterparts. While aged LBT4 sample shows a symmetric hysteresis loop at 30 °C, there is significant pinching in the hysteresis loops of LBT6 and LBT8 already at 30 °C. Hysteresis loops became more pinched with the increasing Li^+ content similar to the case in the fresh samples.

Aging behavior is explained by the symmetry conforming tendency of defect dipoles. Aging mechanism of Li doped $BaTiO_3$ is schematically described in Fig. 5. Upon air quenching of the samples from 200 °C to room temperature, the symmetry of the material changes from paraelectric cubic to ferroelectric tetragonal

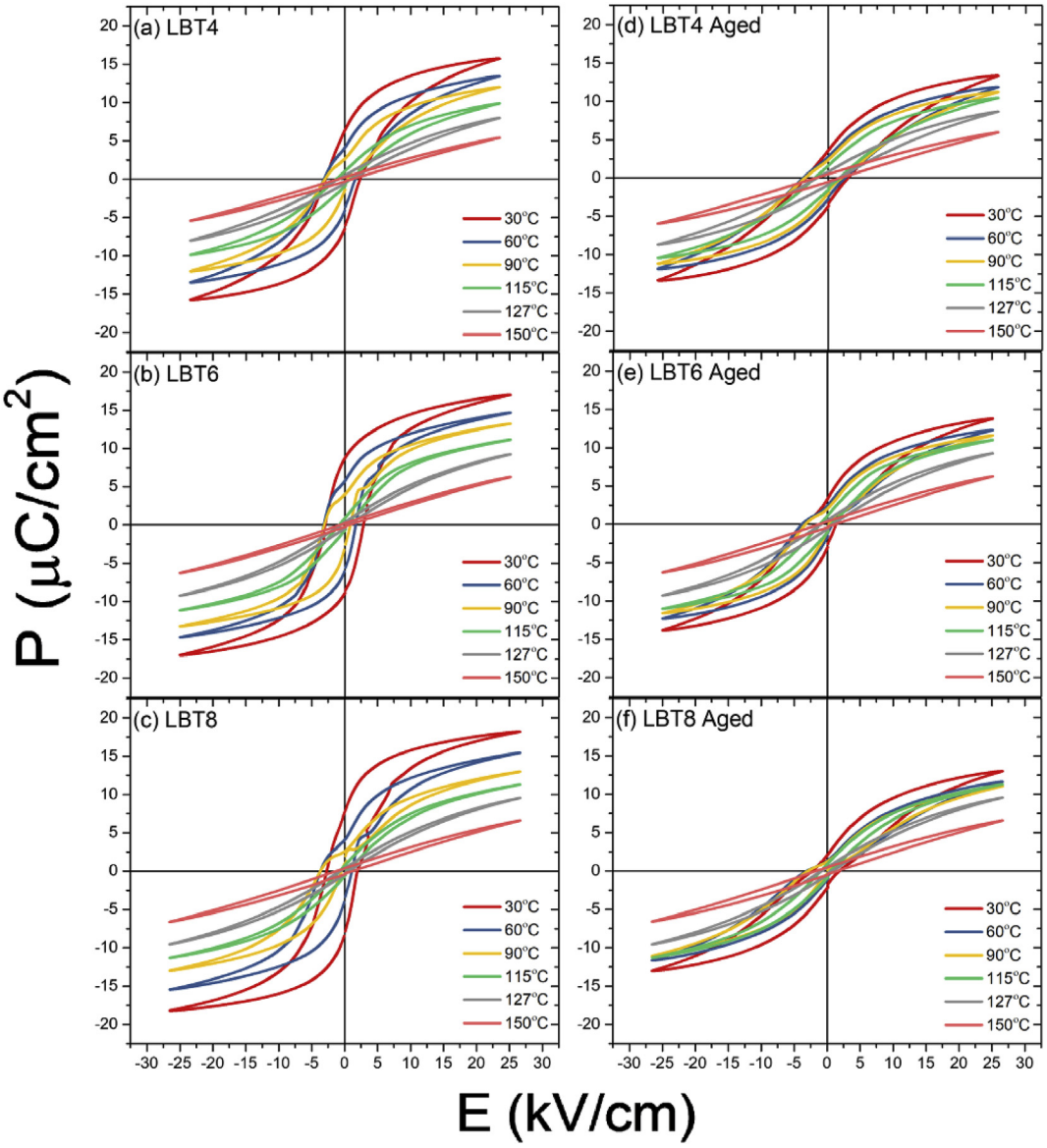

Fig. 4. Ferroelectric hysteresis loops at the different temperatures of fresh LBT ((a), (b), (c)) ceramics and aged BLT ((d), €, (f)) ceramics under 2 kV electric field at 10 Hz.

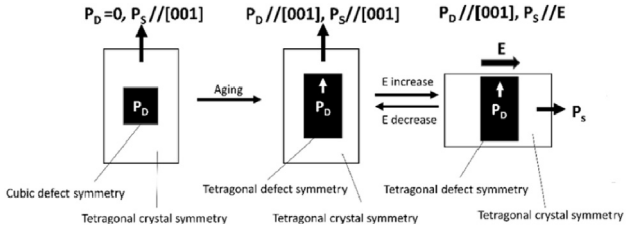

Fig. 5. Aging mechanism for Li-doped $BaTiO_3$ ceramics.

symmetry while the defect symmetry remains cubic due to the slow rate of the oxygen vacancy migration in the lattice. The defect symmetry gradually matches with the material's tetragonal crystal symmetry at room temperature because of symmetry conforming tendency of defects, resulting in aging. When aging occurs polar tetragonal defect symmetry creates a defect polarization, which aligns along the spontaneous polarization (P_S) direction. P_D cannot change its direction with the applied electric field, but the P_S is switched in the direction of the applied electric field, as depicted in Fig. 5 [44]. P_D, being unable to switch its polarization direction under applied electric field, therefore, has a different polarization direction than Ps, acts as an internal field and decreases saturation polarization. This decrease in saturation polarization in aged samples can be seen in Fig. 4. Furthermore, aging induced pinning effect of defect dipoles can induce hysteresis loop pinching or even double hysteresis loops that resemble antiferroelectric behavior [40,44,45].

The temperature dependence of electrical polarization (P(T)) of both fresh and aged LBT ceramics at 20 kV/cm are plotted in Fig. 6. Below T_C, aged samples have lower polarization than fresh samples due to the suppression effect of the defect dipoles according to the SC-SRO principle. When the temperature increases to the phase transition temperature (*Tc*), the ferroelectric microdomains at high temperature weaken the pinning force of the defects [26]. Hence, P(T) curves of fresh and aged samples nearly overlap at and above *Tc* as shown in Fig. 6. The suppression of polarization in the aged

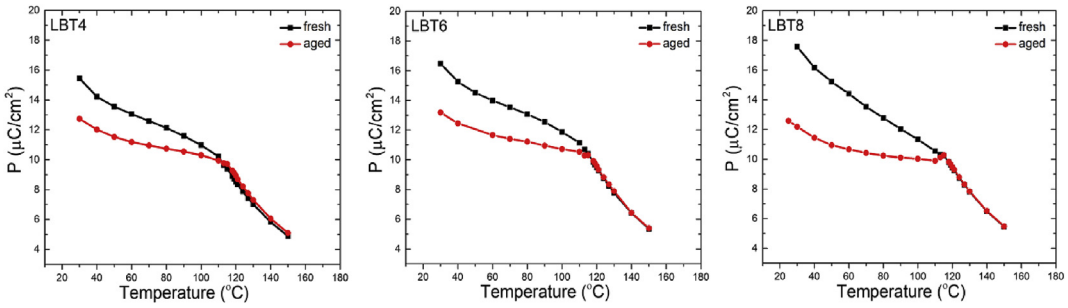

Fig. 6. The temperature dependence of the electrical polarization of fresh and aged LBT4, LBT6, LBT8 ceramics.

samples below T_C will be responsible from the increase of ΔT the as we will discuss below.

In order to evaluate ECE, Maxwell's equations (indirect method) are used. This method is based on the adiabatic reversible process [54], and the electrocaloric temperature change is expressed as:

$$\Delta T = -\frac{1}{\rho}\int_{E_1}^{E_2}\frac{T}{c_p}\left(\frac{\partial P}{\partial T}\right)_E dE \quad (2)$$

In this equation, P is the electrical polarization, T is the temperature, ρ is the density, c_p is the specific heat capacity and E_2, E_1 are final and initial external electric field, respectively. In the calculations, the E_1 and E_2 were taken as zero and 20 kV/cm, respectively. ρ was measured by Archimedes method as 5.48 g/cm^3, 5.47 g/cm^3, 5.40 g/cm^3 for LBT4, LBT6 and LBT8 ceramics, respectively. c_p was assumed as 500 J/(kg K) between 30 °C and 150 °C [55].

We calculated $\left(\frac{\partial P}{\partial T}\right)_E$ by using the small linear increments formula given below in order to avoid having to assume a polynomial fit [56]:

$$\left(\frac{\partial P}{\partial T}\right)_E = \left(\frac{1}{2}\right)\left(\frac{P_n - P_{n-1}}{T_n - T_{n-1}} + \frac{P_{n+1} - P_n}{T_{n+1} - T_n}\right) \quad (3)$$

In Fig. 7, calculated ΔT curves as a function of the temperature are plotted. All fresh and aged LBT ceramics show a peak in ΔT around the Curie temperature. ΔT for fresh samples was calculated as 0.54, 0.57 and 0.53 K under 20 kV/cm for the LBT4, LBT6 and LBT8 samples, respectively. Peak ΔT value increased in aged samples compared to fresh counterparts. This increase amounts to 14.0, 11.0 and 23.5% for LBT4, LBT6 and LBT8, respectively. Aged LBT8 sample behaves differently compared to other two aged compositions. First negative and then positive electrocaloric effect was observed close to T_C, which is due to the slight increase of polarization just below T_C followed by further decrease of polarization above T_C, as can be seen in Fig. 6. We suggest that, for LBT8 sample, where the defect dipoles exceed a critical concentration, defect polarization suppresses the saturation polarization more strongly than in LBT4 and LBT6 samples which is responsible from the slight increase in polarization just below T_C, producing a negative electrocaloric effect. As reported previously, when the temperature increases close to the phase transition temperature, the defect dipoles lose their effectiveness and the material returns to the fresh state polarization [40]. When the effect of defect dipoles is lost close to T_C, the polarization of the LBT8 sample, which has the largest amount of defect dipoles, recovers its fresh state polarization with a slight increase as can be seen in Fig. 7 and also from P-E loops for LBT8 sample between 100° to 115 °C in Fig. 8.

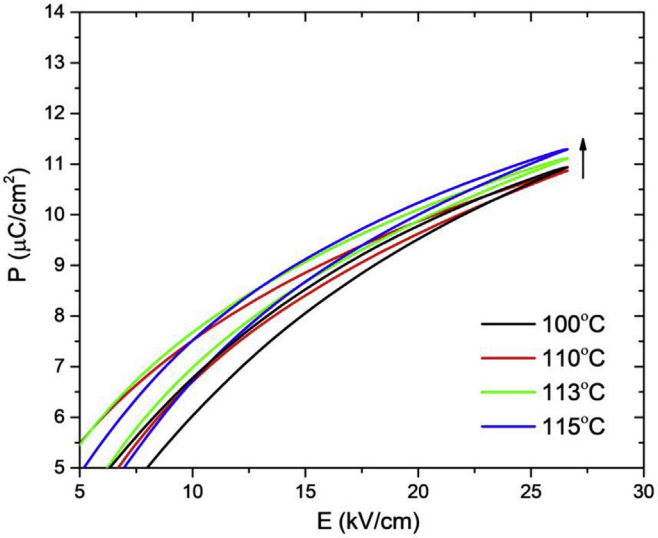

Fig. 8. Ferroelectric hysteresis loops between 100 and 115 °C for the LBT8 samp.

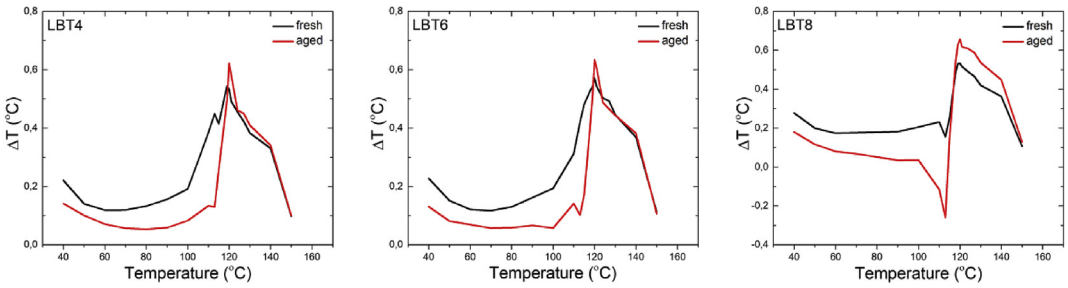

Fig. 7. The temperature dependence of the electrocaloric temperature change (ΔT) under 20 kV/cm for LBT4, LBT6, LBT8 ceramics.

4. Conclusions

In summary, we show that Li^+ doping induced defect polarization have a significant effect on the ECE in LBT ceramics. Defect polarization causes suppression of the saturation polarization below T_C due to the aging effect which increases with increasing Li^+ content. This suppression in aged samples is neutralized close to and above T_C. Polarization change close to T_C becomes sharper in aged samples due to this suppression. As a result, ΔT of aged LBT4, LBT6, and LBT8 samples increases at T_C. Furthermore, in LBT8 sample, both negative and positive ECE were observed. This study shows that electrocaloric effect can be engineered by the utilization of appropriate defect strategies.

Appendix A. Supplementary data

Supplementary data to this article can be found online at https://doi.org/10.1016/j.jallcom.2019.03.356.

References

[1] J.F. Scott, Electrocaloric materials, Annu. Rev. Mater. Res. 41 (2011) 229–240.
[2] M. Ožbolt, A. Kitanovski, J. Tušek, A. Poredoš, Electrocaloric refrigeration: thermodynamics, state of the art and future perspectives, Int. J. Refrig. 40 (2014) 174–188.
[3] S.B. Lang, Cryogenic refrigeration utilizing the electrocaloric effect in pyroelectric lithium sulfate monohydrate, Ferroelectrics 11 (1976) 519–523.
[4] S.-G. Lu, Q. Zhang, Electrocaloric materials for solid-state refrigeration, Adv. Mater. 21 (2009) 1983–1987.
[5] C. Aprea, A. Greco, A. Maiorino, C. Masselli, Solid-state refrigeration: a comparison of the energy performances of caloric materials operating in an active caloric regenerator, Energy 165 (2018) 439–455.
[6] U. Plaznik, M. Vrabelj, Z. Kutnjak, B. Malic, B. Rozic, A. Poredos, A. Kitanovski, Numerical modelling and experimental validation of a regenerative electrocaloric cooler, Int. J. Refrig. 98 (2019) 139–149.
[7] P. Blumenthal, A. Raatz, Classification of electrocaloric cooling device types, Europhys. Lett. 115 (2016) 17004.
[8] A.S. Mischenko, Q. Zhang, J.F. Scott, R.W. Whatmore, N.D. Mathur, Giant electrocaloric effect in thin-film $PbZr_{0.95}Ti_{0.05}O_3$, Science 311 (2006) 1270–1271.
[9] X. Moya, E. Stern-Taulats, S. Crossley, D. González-Alonso, S. Kar-Narayan, A. Planes, L. Mañosa, N.D. Mathur, Giant electrocaloric strength in single-crystal $BaTiO_3$, Adv. Mater. 25 (2013) 1360–1365.
[10] J. Li, D. Zhang, S. Qin, T. Li, M. Wu, D. Wang, Y. Bai, X. Lou, Large room-temperature electrocaloric effect in lead-free $BaHf_xTi_{1-x}O_3$ ceramics under low electric field, Acta Mater. 115 (2016) 58–67.
[11] X.Q. Liu, T.T. Chen, Y.J. Wu, X.M. Chen, M. Valant, Enhanced electrocaloric effects in spark plasma-sintered $Ba_{0.65}Sr_{0.35}TiO_3$-based ceramics at room temperature, J. Am. Ceram. Soc. 96 (2013) 1021–1023.
[12] Y. Bai, X. Han, X.-C. Zheng, L. Qiao, Y. Bai, X.-C. Zheng, X. Han, L. Qiao, Both high reliability and giant electrocaloric strength in $BaTiO_3$ ceramics, Sci. Rep 3 (2013) 2895.
[13] H. Kaddoussi, A. Lahmar, Y. Gagou, B. Asbani, J.L. Dellis, G. Cordoyiannis, B. Allouche, H. Khemakhem, Z. Kutnjak, E.M. Marssi, Indirect and direct electrocaloric measurements of $(Ba_{1-x}Ca_x)(Zr_{0.1}Ti_{0.9})O_3$ ceramics (x = 0.05, x = 0.20), J. Alloys Compd. 667 (2016) 198–203.
[14] H.-J. Ye, X.-S. Qian, J. Lu, H. Gu, S. Zhang, Q.M. Zhang, D.-Y. Jeong, W.-Z. Shao, L. Zhen, Dielectric and electrocaloric responses of $Ba(Zr_{0.2}Ti_{0.8})O_3$ bulk ceramics and thick films with sintering aids, IEEE Trans. Dielectr. Electr. Insul. 22 (2015) 1–5.
[15] X.-S. Qian, H.-J. Ye, Y.-T. Zhang, H. Gu, X. Li, C.A. Randall, Q.M. Zhang, Giant electrocaloric response over a broad temperature range in modified $BaTiO_3$ ceramics, Adv. Funct. Mater. 24 (2014) 1300–1305.
[16] Y. Bai, F. Han, S. Xie, J.T. Li, S.Q. Qin, J.J. Li, L.J. Qiao, D. Guo, Thickness dependence of electrocaloric effect in high-temperature sintered $Ba_{0.8}Sr_{0.2}TiO_3$ ceramics, J. Alloys Compd. 736 (2018) 57–61.
[17] S. Liu, Q. Xie, L. Zhang, Y. Zhao, X. Wang, P. Mao, J. Wang, X. Lou, Tunable electrocaloric and energy storage behavior in the Ce, Mn hybrid doped $BaTiO_3$ ceramics, J. Eur. Ceram. Soc. 38 (2018) 4664–4669.
[18] S.M. Zeng, X.G. Tang, Q.X. Liu, Y.P. Jiang, M.D. Li, W.H. Li, Z.H. Tang, Electrocaloric effect and pyroelectric properties in Ce-doped $BaCe_xTi_{1-x}O_3$ ceramics, J. Alloys Compd. 776 (2019) 731–739.
[19] J.F. Qian, P.H. Hu, C. Liu, J.Y. Jiang, Z.K. Dan, J. Ma, Y.H. Lin, C.W. Nan, Y. Shen, High electrocaloric cooling power of relaxor ferroelectric $BaZr_xTi_{1-x}O_3$ ceramics within broad temperature range, Sci. Bull. 63 (2018) 356–361.
[20] B. Asbani, Y. Gagou, M. Trcek, J.L. Dellis, M. Amjoud, A. Lahmar, D. Mezzane, Z. Kutnjak, M. El Marssi, Dielectric permittivity enhancement and large electrocaloric effect in the lead free $(Ba_{0.8}Ca_{0.2})_{1-x}La_{2x/3}TiO_3$ ferroelectric ceramics, J. Alloys Compd. 730 (2018) 501–508.
[21] K.S. Srikanth, S. Patel, R. Vaish, Electrocaloric behavior and temperature dependent scaling of dynamic hysteresis of $Ba_xSr_{1-x}TiO_3$ (x = 0.7, 0.8 and 0.9) bulk ceramics, J. Australas. Ceram. Soc. 54 (2017) 439–450.
[22] X.Q. Liu, T.T. Chen, M.S. Fu, Y.J. Wu, X.M. Chen, Electrocaloric effects in spark plasma sintered $Ba_{0.7}Sr_{0.3}TiO_3$-based ceramics: effects of domain sizes and phase constitution, Ceram. Int. 40 (2014) 11269–11276.
[23] Y. Hou, L. Yang, X. Qian, T. Zhang, Q.M. Zhang, Electrocaloric response near room temperature in Zr- and Sn-doped $BaTiO_3$ systems, Phil. Trans. R. Soc. A 374 (2016) 20160055.
[24] H. Kaddoussi, A. Lahmar, Y. Gagou, B. Manoun, J.N. Chotard, J.L. Dellis, Z. Kutnjak, H. Khemakhem, B. Elouadi, E.M. Marssi, Sequence of structural transitions and electrocaloric properties in $(Ba_{1-x}Ca_x)(Zr_{0.1}Ti_{0.9})O_3$ ceramics, J. Alloys Compd. 713 (2017) 164–179.
[25] B. Asbani, Y. Gagou, J.L. Dellis, A. Lahmar, M. Amjoud, D. Mezzane, Z. Kutnjak, E.M. Marssi, Structural, dielectric and electrocaloric properties in lead-free Zr-doped $Ba_{0.8}Ca_{0.2}TiO_3$ solid solution, Solid State Commun. 237 (2016) 49–54.
[26] K.S. Srikanth, R. Vaish, Enhanced electrocaloric, pyroelectric and energy storage performance of $BaCe_xTi_{1-x}O_3$ ceramics, J. Eur. Ceram. Soc. 37 (2017) 3927–3933.
[27] L. Zhao, X.Q. Ke, Z.J. Zhou, X.Q. Liao, J.J. Li, Y. Wang, M. Wu, T.Y. Li, Y. Bai, X.B. Ren, Large electrocaloric effect over a wide temperature range in $BaTiO_3$-modified lead-free ceramics, J. Mater. Chem. C 7 (2019) 1353–1358.
[28] F. Han, Y. Bai, L.-J. Qiao, D. Guo, A systematic modification of the large electrocaloric effect within a broad temperature range in rare-earth doped $BaTiO_3$ ceramics, J. Mater. Chem. C 4 (2016) 1842–1849.
[29] Z. Xu, H. Qiang, Enhanced electrocaloric effect in Mn+Y co-doped BST ceramics near room temperature, Mater. Lett. 191 (2017) 57–60.
[30] T. Kimura, Q. Dong, S. Yin, T. Hashimoto, A. Sasaki, T. Sato, Synthesis and piezoelectric properties of Li-doped $BaTiO_3$ by a solvothermal approach, J. Eur. Ceram. Soc. 33 (2013) 1009–1015.
[31] C.A. Randall, S. Wang, D. Laubscher, J.P. Dougherty, W. Huebner, Structure property relationships in core-shell $BaTiO_3$–LiF ceramics, J. Mater. Res. 8 (1993) 871–879.
[32] Q. Lou, X. Shi, X. Ruan, J. Zeng, Z. Man, L. Zheng, C. Park, G. Li, Ferroelectric properties of Li-doped $BaTiO_3$ ceramics, J. Am. Ceram. Soc. 101 (2018) 3597–3604.
[33] N. Ma, B.-P. Zhang, W.-G. Yang, Low-temperature sintering of Li_2O-doped $BaTiO_3$ lead-free piezoelectric ceramics, J. Electroceram. 28 (2012) 275–280.
[34] A. Grünebohm, T. Nishimatsu, Influence of defects on ferroelectric and electrocaloric properties of $BaTiO_3$, Phys. Rev. B 93 (2016) 134101.
[35] Y.-B. Ma, A. Grünebohm, K.-C. Meyer, K. Albe, B.-X. Xu, Positive and negative electrocaloric effect in $BaTiO_3$ in the presence of defect dipoles, Phys. Rev. B 94 (2016) 094113.
[36] T.D. Zhang, W.L. Li, Y.F. Hou, Y. Yu, W.P. Cao, Y. Feng, W.D. Fei, Positive/negative electrocaloric effect induced by defect dipoles in PZT ferroelectric bilayer thin films, RSC Adv. 6 (2016) 71934–71939.
[37] M. Wu, D.S. Song, G. Vats, S.C. Ning, M.Y. Guo, D.W. Zhang, D.Q. Xue, S.J. Pennycook, X.J. Lou, Defect-controlled electrocaloric effect in $PbZrO_3$ thin films, J. Mater. Chem. C 6 (2018) 10332–10340.
[38] H.M. Qiao, C. He, F.P. Zhuo, Z.J. Wang, X.Z. Li, Y. Liu, X.F. Long, Modulation of electrocaloric effect and nanodomain structure in Mn-doped $Pb(In_{0.5}Nb_{0.5})O_3$-$PbTiO_3$ ceramics, Ceram. Int. 44 (2018) 20417–20426.
[39] F. Weyland, A. Bradesko, Y.B. Ma, J. Koruza, B.X. Xu, K. Albe, T. Rojac, N. Novak, Impact of polarization dynamics and charged defects on the electrocaloric response of ferroelectric $Pb(Zr,Ti)O_3$ ceramics, Energy Technol. 6 (2018) 1519–1525.
[40] Z. Feng, Z. Cheng, D. Shi, S. Dou, Aging effect evolution during ferroelectric-ferroelectric phase transition: a mechanism study, AIP Adv 3 (2013) 062105.
[41] D.C. Lupascu, Y.A. Genenko, N. Balke, Aging in ferroelectrics, J. Am. Ceram. Soc. 89 (2006) 224–229.
[42] Z. Li, H. Fan, Oxygen vacancy-induced aging of Mn-doped $Ba_{0.8}Sr_{0.2}TiO_3$ ceramics in paraelectric and ferroelectric state, Solid State Ionics 180 (2009) 1139–1142.
[43] W.A. Schulze, K. Ogino, Review of literature on aging of dielectrics, Ferroelectrics 87 (1988) 361–377.
[44] W. Liu, W. Chen, L. Yang, L. Zhang, Y. Wang, C. Zhou, S. Li, X. Ren, Ferroelectric aging effect in hybrid-doped $BaTiO_3$ ceramics and the associated large recoverable electrostrain, Appl. Phys. Lett 89 (2006) 172908.
[45] P.V. Lambeck, G.H. Jonker, The nature of domain stabilization in ferroelectric perovskites, J. Phys. Chem. Solids 47 (1986) 453–461.
[46] T. Granzow, E. Suvaci, H. Kungl, M.J. Hoffmann, Deaging of heat-treated iron-doped lead zirconate titanate ceramics, Appl. Phys. Lett 89 (2006) 262908.
[47] K. Uchino, Ferroelectric Devices, second ed., CRC Press, 2009.
[48] X. Ren, Large electric-field-induced strain in ferroelectric crystals by point-defect-mediated reversible domain switching, Nat. Mater. 3 (2004) 91–94.
[49] L.X. Zhang, X. Ren, In situ observation of reversible domain switching in aged Mn-doped $BaTiO_3$ single crystals, Phys. Rev. B 71 (2005) 174108.
[50] L.X. Zhang, W. Chen, X. Ren, Large recoverable electrostrain in Mn-doped (Ba,Sr) TiO_3 ceramics, Appl. Phys. Lett. 85 (2004) 5658–5660.
[51] B.H. Toby, R.B. Von Dreele, GSAS-II: the genesis of a modern open-source all purpose crystallography software package, J. Appl. Crystallogr. 46 (2013) 544–549.
[52] Y.D. Hou, L.M. Chang, M.K. Zhu, X.M. Song, H. Yan, Effect of Li_2CO_3 addition on the dielectric and piezoelectric responses in the low-temperature sintered

0.5PZN-0.5PZT systems, J. Appl. Phys. 102 (2007) 084507.
[53] D.D. William, L. Warren, Rainer M. Waser, Degradation mechanisms in ferroelectric and high-permittivity perovskites, MRS Bull. 21 (1996) 40–45.
[54] P.D. Thacher, Electrocaloric effects in some ferroelectric and antiferroelectric $Pb(Zr,Ti)O_3$ compounds, J. Appl. Phys. 39 (1968) 1996–2002.
[55] Y. He, Heat capacity, thermal conductivity, and thermal expansion of barium titanate-based ceramics, Thermochim. Acta 419 (2004) 135–141.
[56] F.L. Goupil, A. Berenov, A.-K. Axelsson, M. Valant, N.M. Alford, Direct and indirect electrocaloric measurements on $\langle 001 \rangle PbMg_{1/3}Nb_{2/3}O_3-30PbTiO_3$ single crystals, J. Appl. Phys. 111 (2012) 124109.